Ocean Colour Climate Change Initiative (OC_CCI) - Phase One

ATBD v1 - Polymer atmospheric correction algorithm

Ref: D2.3

Date: 25/10/12

Issue: 1.3

For: ESA / ESRIN

PML Plymouth Marine Laboratory

VEGA Helmholtz-Zentrum Geesthacht Centre for Materials and Coastal Research Brockmann Consult JRC European Commission HYGEOS NERSC

This Page is Intentionally Blank

SIGNATURES AND COPYRIGHT

Project : **Ocean Colour Climate Change Initiative (OC_CCI) - Phase One**

Document Title: **ATBD v1 -** Polymer atmospheric correction algorithm

Reference : **D2.3**

Issued : **Oct. 25, 2012**

Issue : **1.3**

Client : **ESA / ESRIN**

Authored : 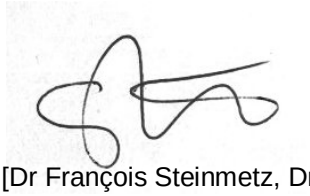
[Dr François Steinmetz, Dr Didier Ramon, Dr Pierre-Yves Deschamps – Hygeos]

Approved : 
[Dr Frederic Melin - JRC, Dr Carsten Brockmann - BC, John Swinton – Telespazio VEGA, Dr Shubha Sathyendranath - PML]

Approved : 
[Dr Shubha Sathyendranath - PML]

Address : Plymouth Marine Laboratory (PML)
Prospect Place
The Hoe
Plymouth PL1 2DH
United Kingdom
Tel: +44 (0)1752 - 633100

Document Change Log

Issue/ Revision	Date	Comment
v0	Jan 31, 2011	
v1	Apr 10, 2012	Update to sections 4.2, 4.3: update of the reflectance model, modification for hyperoligotrophic waters, water bidirectional reflectance and “full” normalization of reflectances.
v1.1	May 04, 2012	Rewritten section 6 (uncertainty estimation) with updated method and new results.
v1.2	Sept. 05, 2012	Updated sections 4.3 and 4.4 (definition of the chi-square quantity)
V1.3	Oct. 25, 2012	Removed section “uncertainty estimation”

This Page is Intentionally Blank

TABLE OF CONTENTS

1. INTRODUCTION 9

2. DECOMPOSITION OF THE TOA SIGNAL 10

2.1 TOA reflectance 10
2.2 Gaseous absorption 10
2.3 Rayleigh scattering and initial sun glint correction 10
2.4 Look-up tables description 12
2.5 Workflow 13

3. CLOUD MASKING 15

3.1 Basic cloud mask 15
3.2 Advanced cloud mask 15
3.3 Cloud mask based on O2 pressure 16

4. SPECTRAL MATCHING 18

4.1 Atmosphere and sun glint model 18
4.2 Water reflectance model 19
4.2.1 Description 19
4.2.2 Adjustment of the absorption coefficient for oligotrophic waters 21
4.3 Optimization method 23
4.4 Workflow 27

5. SENSITIVITY STUDY 28

6. IMPLEMENTATION CONSIDERATIONS 32

6.1 Language, system and libraries 32
6.2 Computation time 32
6.3 Input data 32
6.4 Output data 33

7. REFERENCES 35

INDEX OF TABLES

Table 1: Parameters for the look-up table “LUT_MOL_GLI_R” 12

Table 2: Parameters for the look-up table “LUT_MOL_GLI_T” 12

Table 3: Parameters for the look-up table “LUT_MOL_R” 13

Table 4: libraries used by Polymer 32

Table 5: List of Polymer input formats 32

Table 6: List of Polymer output datasets 33

INDEX OF FIGURES

Figure 1: Workflow for the initial corrections 14

Figure 2: Examples of spectra for the model of water reflectances used in Polymer. It is based on two parameters: the chlorophyll concentration (chl) and the backscattering coefficient of suspended matter ($\boldsymbol{bbNC}$). On Fig. (a), $\boldsymbol{bbNC}$ is set to zero, and thus corresponds between 350 and 700 nm to the model by (Morel & Maritorena, 2001) (solid curve). It is extended from 700 to 900 nm using the similarity spectrum for turbid waters (Ruddick, Cauver, & Park, 2006) (dashed curves). Fig. (b) shows how the spectrum varies with the parameter $\boldsymbol{bbNC}$, for two chlorophyll concentrations. 21

Figure 3: plot of the values of $\boldsymbol{Kbio(420)}$ measured during the BIOSOPE campaign. The solid black line represents the empirical relation proposed by (Morel & Maritorena, 2001). Figure from (Morel A. , et al., 2007). The solid blue line is added to the figure, and corresponds to the fit of the measurements. 22

Figure 4: Impact of the adjustment of the water reflectance model on the spectral shape of the reflectances, for different chlorophyll concentrations. The solid lines are without the model adjustment, and the dashed lines include the model adjustment. 23

Figure 5: Seasonal evolution of the mean reflectance at 560 nm over the South Pacific Gyre – without a constraint on the backscattering coefficient (a) and with a constraint (b) 26

Figure 6: Workflow for the spectral matching process 27

Figure 7: Plots for the comparison between the simulated parameters (synthetic dataset, indicated by subscript "sim"), and the parameters retrieved by POLYMER (indicated by subscript "ret"). In these figures, noise has been added to TOA reflectances according to typical Sentinel-3 SNR. Each row corresponds to the following parameters: chlorophyll concentration, water reflectance at 443 nm and 560 nm. The first column (Figs. (a), (d) and (g)) shows the regression between the synthetic and retrieved parameters, for the "mixed" case. The second column (Figs. (b), (e) and (h)) show the relative percent difference, between the retrieved and synthetic values (ret – simsim), as a function of the sun glint reflectance; emphasis is put on the sun glint correction by using the case "no aerosol". The difference between $\boldsymbol{log10(chlret)}$ and $\boldsymbol{log10(chlsim)}$ is multiplied by $\boldsymbol{ln(10)}$ to convert to relative percent difference of the chlorophyll concentration ($\boldsymbol{\Delta chlchl \approx ln10\Delta log10(chl)}$). The third column (Figs. (c), (f) and (i)) shows the relative percent difference, between the retrieved and synthetic values, as a function of the aerosol optical thickness at 865 nm; emphasis is put on the aerosol correction by using the case "no glint". 29

Figure 8: Summary of the relative precision (a) and accuracy (b) of the comparison between synthetic and retrieved water reflectances at each wavelength, for the "mixed" case, with and without noise added to TOA reflectances. GCOS recommends an accuracy of 5% on water reflectance in the blue and green bands. 30

This Page is Intentionally Blank

1. INTRODUCTION

This document describes the atmospheric and sun glint correction algorithm called “Polymer” (POLYnomial based algorithm applied to MERIS). It is based on the paper “Atmospheric correction in presence of sun glint: application to MERIS” (Steinmetz F., 2011). It extends the algorithm description on several topics, such as the cloud mask, implementation consideration and recent modifications to the algorithm.

Polymer was originally developed to process MERIS data, but is being extended to process multiple sensors; currently MODIS is also supported.

2. DECOMPOSITION OF THE TOA SIGNAL

2.1 TOA reflectance

The radiance L_{TOA} measured at wavelength λ at the top of the atmosphere (TOA) with a solar zenith angle θ_s, is converted to reflectances ρ_{TOA} by normalization to extraterrestrial solar irradiance F_0:

$$\rho_{TOA}(\lambda) = \frac{\pi \cdot L_{TOA}(\lambda)}{\cos(\theta_s) \cdot F_0(\lambda)}$$

This reflectance can be decomposed as follows:

$$\rho_{\text{TOA}}(\lambda) = t_{oz}(\lambda) \cdot t_{NO2}(\lambda) \cdot [\rho_{\text{mol}}(\lambda) + T(\lambda)\rho_{\text{gli}} + \rho_{\text{aer}}(\lambda) + \rho_{\text{coupl}}(\lambda) + t(\lambda)\rho_w^+(\lambda)]$$

In this decomposition, $t_{oz}(\lambda)$ is the transmittance of the ozone, $t_{NO2}(\lambda)$ is the transmittance of the nitrogen dioxide, $\rho_{\text{mol}}(\lambda)$ is the Rayleigh scattering, ρ_{gli} is the (non-spectral) sun glint reflectance transmitted by the direct transmission factor $T(\lambda)$, $\rho_{\text{aer}}(\lambda)$ is the reflectance of the aerosols (which are considered non-absorbing), $\rho_{\text{coupl}}(\lambda)$ accounts for the various coupling terms between the sun glint, the molecules and the aerosols, $t(\lambda)$ is the total (direct and diffuse) transmission for atmospheric scattering and $\rho_w^+(\lambda)$ is the water reflectance above the water-air interface.

2.2 Gaseous absorption

The transmittances $t_{oz}(\lambda)$ and $t_{NO2}(\lambda)$ are estimated using the ozone and NO2 columns provided as ancillary data. For MERIS, the total ozone concentration is obtained from ECMWF data (European Centre for Medium-Range Weather Forecasts). For MODIS, it is obtained from NCEP data. The total NO2 is derived from climatology data, following the correction used in MODIS processing (Ahmad, et al., 2007).

2.3 Rayleigh scattering and initial sun glint correction

Pure Rayleigh scattering can be accurately predicted, and corrected; it depends on the observation geometry and atmospheric pressure at sea level P_0. Also, an initial correction for the sun glint is performed: it is estimated from the wind speed meteorological data using the sea surface roughness model by (Cox & Munk, 1954) without including wind direction. The term associated with this initial correction is given by $\rho_{\text{mol+gli}}(\lambda, V_{\text{wind}})$, which includes Rayleigh scattering, the sun glint and the coupling between Rayleigh scattering

and sun glint. This term is interpolated in a look-up table, which is described in section 2.4.

Thus, the initial correction is written as:

$$\rho'(\lambda) = \frac{\rho_{\text{TOA}}(\lambda)}{t_{oz}(\lambda) \cdot t_{NO2}(\lambda)} - \rho_{\text{mol+gli}}(\lambda, V_{\text{wind}})$$

In this initial correction, the wind speed at each pixel is not known accurately; consequently, there can be a large difference (several percents) between the simulated and actual sun glint. Therefore, a mis-estimation of the wind speed will lead to a mis-estimation of $\rho'(\lambda)$, and can possibly lead to negative values of $\rho'(\lambda)$. This is not a problem since only the spectral shape of this term is important in the present atmospheric correction process, rather than its absolute values. The choice of still doing a rough initial correction for the sun-glint is made to remove a significant portion of the sun glint, thus reducing the amplitude of the remaining signal to be corrected for. To account for the inaccuracy of this initial correction, a residue $\Delta\rho_{\text{gli}}(\lambda)$ of sun glint and its coupling with Rayleigh scattering is introduced:

$$\rho_{\text{mol}}(\lambda) + T(\lambda)\rho_{gli} = \rho_{\text{mol+gli}}(\lambda, V_{\text{wind}}) + \Delta\rho_{\text{gli}}(\lambda)$$

Thus, $\rho'(\lambda)$ can be written as:

$$\rho'(\lambda) = \rho_{\text{ag}}(\lambda) + t(\lambda)\rho_w^+(\lambda)$$

where $\rho_{\text{ag}}(\lambda)$ represents the residue of sun-glint, the aerosol scattering and the coupling terms:

$$\rho_{\text{ag}}(\lambda) = \Delta\rho_{\text{gli}}(\lambda) + \rho_{aer}(\lambda) + \rho_{\text{coupl}}(\lambda)$$

Like $\rho_{\text{mol+gli}}$, the term $t(\lambda)$ is pre-calculated with the SOS code and stored in look-up tables (see section 2.4). In this case, the assumption is that the transmission of the aerosols is negligible, which is valid in most cases - when the aerosols are not absorbing. Thus, it is approximated as the transmission factor of an atmosphere containing only molecules, and is calculated under the same conditions as $\rho_{\text{mo+gli}}$. It depends on the following parameters: the sun and sensor zenith angles, the surface pressure and the wind speed.

The objective of the algorithm will be to decompose $\rho'(\lambda)$ into the ocean water scattering $\rho_w^+(\lambda)$ and the signal scattered by the atmosphere and the residual sun glint $\rho_{ag}(\lambda)$.

This decomposition is based on the models described in section 4.

2.4 Look-up tables description

Three look-up tables are used to take into account the Rayleigh scattering in Polymer:

- LUT_MOL_GLI_R: The first one contains $\rho_{mol+gli}$, the reflectance of a simulated atmosphere including only the Rayleigh scattering, the sun glint (wavy sea surface) and their couplings.

Table 1: Parameters for the look-up table "LUT_MOL_GLI_R"

Parameter	Description	Dimension
μ_s	cosine of the solar zenith angle	25
ϕ	relative azimuth angle	37
μ_v	cosine of the viewing zenith angle	25
λ	spectral band	MERIS: 15 MODIS: 10
WS	wind speed	16

Rem: $\rho_{mol+gli}$ is also corrected for the variation of atmospheric pressure. The correction factor is P_{atm}/P_0, where P_{atm} is the atmospheric pressure obtained from meteorological data and P_0 is the standard atmospheric pressure 1013 hPa.

- LUT_MOL_GLI_T: The second one contains the corresponding atmospheric transmission $t(\lambda)$

Table 2: Parameters for the look-up table "LUT_MOL_GLI_T"

Parameter	Description	Dimension
μ_s	cosine of the solar zenith angle	25

λ	spectral band	MERIS: 15 MODIS: 10
WS	wind speed	16

An adjustment for the atmospheric pressure is also performed.

- LUT_MOL_R: The third one contains ρ_{mol} at 865 nm, the reflectance of a simulated atmosphere including only the Rayleigh scattering, without sun glint. It is used for correcting the TOA reflectance for the Rayleigh scattering at 865 nm, for use in the cloud mask calculation (see section 3.1)

Table 3: Parameters for the look-up table "LUT_MOL_R"

Parameter	Description	Dimension
μ_s	cosine of the solar zenith angle	25
ϕ	relative azimuth angle	37
μ_v	cosine of the viewing zenith angle	25
λ	spectral band	MERIS: 15 MODIS: 10

These tables are calculated with the Successive Order of Scattering radiative transfer code (SOS, (Lenoble, Herman, Deuze, Lafrance, Santer, & Tanre, 2007)). All these simulations are performed without aerosols, and by assuming a black surface.

2.5 Workflow

The workflow for the initial corrections described in the previous sections is presented on Figure 1.

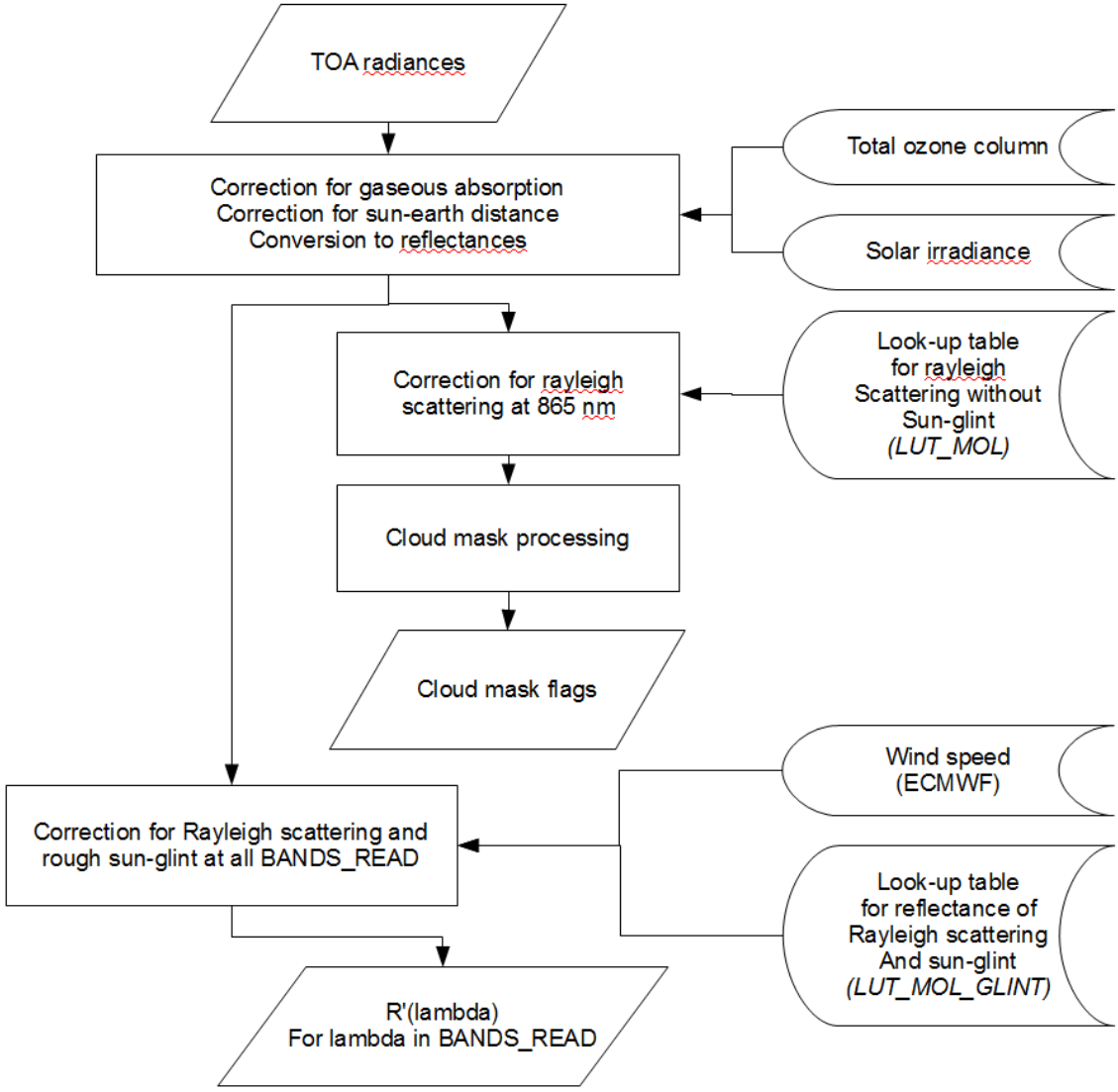

Figure 1: Workflow for the initial corrections

3. CLOUD MASKING

Several flags are proposed for cloud masking. These flags have been developed for MERIS and are currently not used for MODIS processing. Three different cloud masks are implemented:

- when the basic cloud mask is raised, the pixel is not processed
- the other cloud masks are designed to detect weaker cloud contamination, but the corresponding pixels are processed anyway (quality indicator)

The cloud mask that will be used in OC-CCI is a tool called IdePix, developed by Brockmann Consult. It is a more advanced tool based on machine learning of human classified cases, and is expected to be better – this cloud mask embraces the methods described hereafter.

3.1 Basic cloud mask

The basic cloud mask used in Polymer is based on $\rho''(865)$, the TOA reflectance at 865 nm, only corrected for the Rayleigh scattering. This correction does not include an initial sun glint correction.

$$\rho''(865) = \rho_{\text{TOA}}(865) - \rho_{\text{mol}}(865)$$

where $\rho_{\text{mol}}(865)$ is interpolated in the look-up table described in section 2.4.

A pixel (i,j) is flagged out when any of the following two criteria is met:

- $\rho''(865) > T_{\text{cloud}}$ where $T_{\text{cloud}} = 0.2$
- $\text{std}_{3x3}\left(\rho''(865)\right) > S_{\text{cloud}}$ where $S_{\text{cloud}} = 0.04$ and std_{3x3} is the standard deviation over a block of 3 by 3 pixels

The value of T_{cloud} is purposely chosen high, to avoid masking the sun glint.

3.2 Advanced cloud mask

This second cloud mask is designed to filter out thin clouds with a reflectance lower than T_{cloud}. It is based on the reflectance at 865 nm from which the sun glint estimated from the wind speed is subtracted:

$$R_{\text{cloud}} = \rho''(865) - \rho_{\text{gli}}(V_{\text{wind}})$$

In this expression, $\rho_{\text{gli}}(V_{\text{wind}})$ is the sun glint intensity estimated from the ECMWF wind speed using Cox and Munk model (Cox & Munk, 1954). The following thresholds on R_{cloud} are used to obtain two flags:

- $R_{\text{cloud}} > 0.03$
- $R_{\text{cloud}} > 0.05$

Note that in the sun-glint area, non-cloudy pixels may be flagged out if $\rho_{\text{gli}}(V_{\text{wind}})$ is under-estimated; on the contrary, cloudy pixels may not be flagged out if $\rho_{\text{gli}}(V_{\text{wind}})$ is over-estimated. Therefore, these flags should be considered as complementary to other flags.

3.3 Cloud mask based on O2 pressure

Cloud top pressure can be retrieved using MERIS O2 absorption bands (Fisher & Grassl, 1991); this parameter is highly sensitive to the presence of cirrus, and its use as a cloud mask is summarized in this section.

The O2 pressure P_{O_2} can be estimated using a ratio between MERIS bands 761 and 753 nm:

$$P_{O_2} = \sqrt{\frac{10^P}{m^*}}$$

where m^* is the "air mass" $\frac{1}{\cos(\theta_s)} + \frac{1}{\cos(\theta_v)}$ and P is calculated from the following polynomial:

$$P = \sum_{i=0}^{11} p_i \cdot r^k$$

In this expression, r is the ratio between the reflectances at bands 761 and 753:

$$r = \frac{\rho_{\text{TOA}}(761)}{\rho_{\text{TOA}}(753)}$$

and the polynomial coefficients p_i are interpolated in a look-up table according to the actual central wavelength of the 761 band λ_{761} (which varies cross-track).

This parameter is highly sensitive to the wavelength λ_{761}, and a fine-tuning is necessary to avoid large cross-track effects, especially at camera transitions. The following correction factor for the ratio r is proposed:

$$\begin{cases} C = 0.643 \cdot \mathrm{atan}(75 \cdot \rho_{761}) \text{ for camera 4 (detector index between 555 and 739)} \\ C = 0.645 \cdot \mathrm{atan}(65 \cdot \rho_{761}) \text{ otherwise} \end{cases}$$

The determination of this correction factor is described in (Ramon, Cazier, & Santer, 2003).

However, this correction is not perfect, and residual inter-camera transitions remain. To avoid these inter-camera transitions, the cloud mask at each pixel is based on the difference between P_{O_2} and the "clear-sky PO2 value". This clear-sky PO2 value is estimated by calculating the 95th percentile of the P_{O_2} over a block of 15x25 pixels around the considered pixel. Finally, the cloud mask is obtained by a threshold on this difference:

$$\Delta P_{O_2} = P_{O_2} - P_{O_2\,\text{clear-sky}} < -50 \text{ hPa}$$

Since Polymer shows a good robustness to the presence of cirrus, this cloud mask is used as a quality flag in Polymer rather than a rejection criterion. This parameter could also be used as a proxy to estimate the cloud top height, and the contamination by cloud shadows.

4. SPECTRAL MATCHING

4.1 Atmosphere and sun glint model

If we assume that the water reflectance spectrum is known, the reflectance of the residual sun glint, aerosols and couplings $\rho_{ag}(\lambda)$ is numerically given by $\rho'(\lambda) - t(\lambda)\rho_w^+(\lambda)$. The basic principle of the POLYMER algorithm is to model this atmosphere contribution and the residual sun glint as a polynomial with three terms:

$$\rho_{ag}(\lambda) \approx T_0(\lambda)c_0 + c_1\lambda^{-1} + c_2\lambda^{-4}$$

By introducing this model, we do not try to model each individual component among the glitter, the aerosols and the couplings. Instead, we choose to model the various terms of $\rho_{ag}(\lambda)$, as described in section 2.3 as a whole, by the previous polynomial. The coefficients c_0, c_1 and c_2 are estimated by least square fitting of the observation ; the method will be detailed in section 4.

The motivation for this model is that we expect the signal $\rho_{ag}(\lambda)$ to contain the following spectral components:

- spectrally flat components: the residual sun glint, but also the cloud reflectance and the large particle scattering (aerosol coarse mode: maritime aerosols, cloud droplets, dust). A transmission factor $T_0(\lambda)$ is applied to this term, and accounts for the beam attenuation due to Rayleigh scattering (the transmission by aerosols is neglected). In presence of sun glint (a specular target), this transmission is the direct transmission, which is given by:

  $$T_0^{\text{dir}}(\lambda) = \exp[-\tau_m(\lambda) \times (\frac{1}{\mu_s} + \frac{1}{\mu_v})]$$

  In this expression, μ_s and μ_v are the cosines of the solar and view zenith angles, and the Rayleigh optical thickness $\tau_m(\lambda) \approx 0.00877\lambda^{-4.05}$, with λ in nm. In presence of a lambertian target (cloud droplets, maritime aerosols), the diffuse transmission can be approximated by:

  $$T_0^{\text{dif}}(\lambda) = \exp[-\frac{\tau_m(\lambda)}{2} \times (\frac{1}{\mu_s} + \frac{1}{\mu_v})]$$

The predicted reflectance of the sun glint (using wind data from ECMWF) is used to switch between the direct (in the sun glint, where $\rho_{gli} > \rho_{gli,0}$, with $\rho_{gli,0}$ = 2%) and diffuse (outside sun glint, where $\rho_{gli} < \rho_{gli,0}$) transmission factors:

$$T_0^{tot}(\lambda) = \exp\left[-\tau_m(\lambda) \times \left(1 - \frac{1}{2}\exp\left(-\frac{\rho_{gli}}{\rho_{gli,0}}\right)\right) \times \left(\frac{1}{\mu_s} + \frac{1}{\mu_v}\right)\right]$$

- the aerosol signal, with a spectral dependency (Angstrom coefficient) in the order of -1 (aerosol fine mode),
- the couplings between flat components and the Rayleigh scattering, with a spectral dependency in the order of -4.

The actual spectral dependencies of these various components can vary, for example the aerosols Angstrom coefficient can vary from less than \$0.2\$ to more than \$1.5\$. Also, a transmission factor applies to the spectrally flat sun glint, and, to a lesser extent, to the scattering of semi-transparent clouds. These variations of spectral dependency will be automatically taken into account in the polynomial fitting process, leading to a balance between the three terms c_0, c_1 and c_2.

It is worthwhile to note that in this model, the wavelength λ is the central wavelength for the considered band; for MERIS, this wavelength is known to vary cross-track (this is often referred to as the "smile effect"). This variation is larger than 1 nm at all bands, and leads to large errors in the retrieval of ocean color parameters, if not taken into account. This effect is generally corrected at level 1 by a linear interpolation technique (D'Alba & Colagrande, 2005). Instead, we chose in POLYMER to keep the level 1 raw reflectances (not corrected for the smile effect), and to use for each pixel the exact central wavelength in the atmospheric correction process.

4.2 Water reflectance model

4.2.1 Description

The bio-optical water reflectance model used in the atmospheric correction process uses two parameters: the chlorophyll concentration and the backscattering coefficient of noncovarying particles $b_{bNC}(\lambda)$; it is taken just above the surface and will be noted $\rho^{+}_{wmod}(\text{chl}, b_{bNC}, \lambda)$. The spectrum has been modeled according to Morel (1988), including the updates from Morel & Maritorena (2001). Following Morel et al (2007), the scattering coefficient of pure water $b_w(\lambda)$ is taken from Buiteveld, Hakvoort, & Donze (1994), and multiplied by a factor 1.3 to account for the increase of scattering due to the presence of salts in the ocean water.

The expression of the water bidirectional reflectance above the surface, between 300 and 700 nm, is given by:

$$\rho^{+}_{wMM}(\lambda) = \pi \frac{f}{Q} \frac{(1-\rho)(1-\bar{\rho})}{n_w^2} \frac{b_b}{a}$$

where $\frac{f}{Q}$ is the bidirectional water reflectance factor given in (Morel & Gentili, 1993) and depends on the chlorophyll concentration, the wavelength and the observation geometry; ρ is the surface reflectance for upward radiance, $\bar{\rho}$ is the surface reflectance for downward irradiance, n_w is the refractive index of seawater, b_b is the total backscattering coefficient and a the absorption coefficient.

The backscattering coefficient of noncovarying particles $b_{bNC}(\lambda)$ has been added to the total backscattering coefficient. The spectral dependency for this term has been chosen to be λ^{-1}: the total backscattering coefficient becomes:

$$b_b(\lambda) = \frac{1}{2} b_w(\lambda) + b_{bp}(\lambda) + b_{bNC}(\lambda)$$

There are several reasons for adding this variable backscattering coefficient:

1. even in case 1 waters, there is a large variability of the total backscattering coefficient around the mean b_{bp}-to-chl relationship (Loisel & Morel, 1998). Notably, if this variability is not taken into account, the retrieved reflectances at 510 nm are almost constant, which is anomalous, and has been verified on in-situ data (but not detailed in this paper for brevity). More generally, we have verified that there is a better fit between the reflectances estimated by POLYMER and *in-situ* data when this variable parameter is introduced.
2. Even though the algorithm is not primarily targeted at case 2 waters, the presence of the variable backscattering coefficient makes it possible to behave correctly in coastal waters. Without this coefficient, anomalous reflectances are retrieved, with values decreasing toward the coast at all bands. This term being introduced, the iterative scheme described by Morel & Maritorena (2001) is followed to generate the modified spectrum.

This model has also been extended from 700 nm to 900 nm, by using the similarity spectrum for turbid waters (Ruddick, Cauver, & Park, 2006): the similarity spectrum is normalized at 700 nm to ensure continuity at this wavelength:

$$\rho^{+}_{wmod}([\text{chl}], b_{bNC}, \lambda) = \begin{cases} \rho^{+}_{\text{wMM}}([\text{chl}], \text{b}_{\text{bNC}}, \lambda) & [\lambda < 700\text{nm}] \\ \rho^{+}_{\text{wS}}(\lambda)\rho^{+}_{\text{wMM}}([\text{chl}], \text{b}_{\text{bNC}}, 700\text{nm})/\rho^{+}_{\text{wS}}(700\text{nm}) & [\lambda \geq 700\text{nm}] \end{cases}$$

The resulting spectra are presented on Figs. Figure 2(a) and Figure 2(b). Fig. Figure 2(a) shows the spectrum of case 1 waters, and its extension up to 900 nm using the similarity spectrum (the two spectra overlap between 650 and 700 nm). In the range 700 to 900 nm, a very similar spectrum is obtained when using the reciprocal of the pure water absorption coefficient ($1/a_w(\lambda)$), as demonstrated in Ruddick et al (2006). Fig. Figure 2(b) shows the modeled spectra for two chlorophyll concentrations and three values of b_{bNC}: the latter parameter introduces an offset on the spectrum, but does not change significantly its shape.

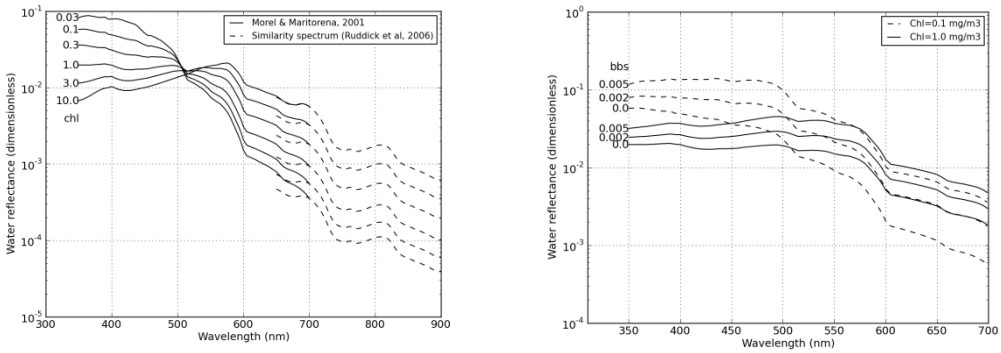

(a) (b)

Figure 2: Examples of spectra for the model of water reflectances used in Polymer. It is based on two parameters: the chlorophyll concentration (chl) and the backscattering coefficient of suspended matter (b_{bNC}). On Fig. (a), b_{bNC} is set to zero, and thus corresponds between 350 and 700 nm to the model by (Morel & Maritorena, 2001) (solid curve). It is extended from 700 to 900 nm using the similarity spectrum for turbid waters (Ruddick, Cauver, & Park, 2006) (dashed curves). Fig. (b) shows how the spectrum varies with the parameter b_{bNC}, for two chlorophyll concentrations.

4.2.2 Adjustment of the absorption coefficient for oligotrophic waters

A modification was introduced to the water reflectance model, to better represent oligotrophic waters. This modification follows (Morel A. , et al., 2007), which noticed

during the campaign BIOSOPE the underestimation of the reflectances of very oligotrophic waters in the blue,

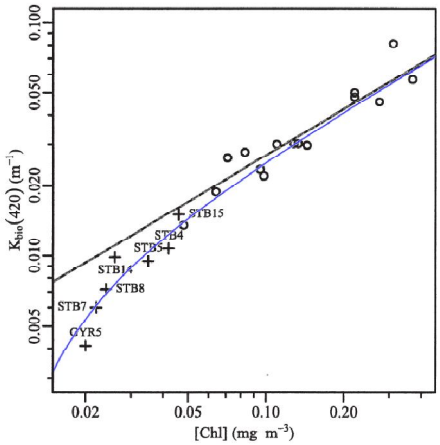

Figure 3: plot of the values of $K_{bio}(420)$ measured during the BIOSOPE campaign. The solid black line represents the empirical relation proposed by (Morel & Maritorena, 2001). Figure from (Morel A. , et al., 2007). The solid blue line is added to the figure, and corresponds to the fit of the measurements.

The values of $K_{bio(420)}$ is associated to the presence of non-algal particles and dissolved material, so we choose to add the following (negative) term, with a spectral shape S_{nap} = 0.011 (Bricaud A., 1998):

$$a_{nap}(\text{chl}, \lambda) = -\exp(-7.55 \cdot \text{chl}^{0.08}) \cdot \exp(-S_{nap} \cdot (\lambda - 420))$$

The first factor in this expression corresponds to the blue curve on Figure 3, and the second term is the spectral dependency term. This term a_{nap} is added to the absorption coefficient as described previously.

The impact of this modification is shown on Figure 4. We can see the increase of the reflectances in the blue, in the case of clear waters.

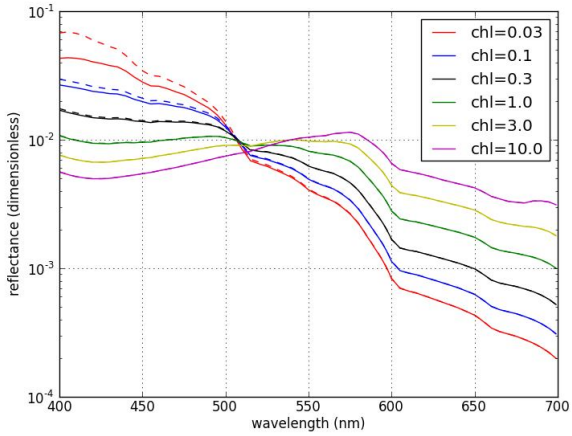

Figure 4: Impact of the adjustment of the water reflectance model on the spectral shape of the reflectances, for different chlorophyll concentrations. The solid lines are without the model adjustment, and the dashed lines include the model adjustment.

4.3 Optimization method

The goal of the POLYMER algorithm is to use the two models previously described, to separate the signal $\rho_{ag}(\lambda)$, from the signal scattered by the sea water. The whole range of available spectral bands can be used for this process. This technique of spectral matching consists in optimizing the parameters of the atmospheric model (c_0, c_1 and c_2) and the parameters of the ocean water reflectance model ([chl] and b_{bNC}), in order to obtain the best spectral fit of $\rho'(\lambda)$. In this scheme, a subset of N bands ($\lambda_1, \ldots, \lambda_N$) in all available spectral bands is used. It is theoretically possible to use any subset of the available bands, with a minimum of N=5 bands corresponding to the number of parameters.

MERIS instrument has 15 bands, and we have discarded 5 of them: 681 (chlorophyll fluorescence peak), 709 (imprecise correction for water vapour absorption), 760 (oxygen absorption band), 885 and 900 nm (reduced signal-to-noise). Therefore the following N=10 remaining bands are used: 412, 443, 490, 510, 560, 620, 665, 754, 779 and 865 nm.

For MODIS processing, the following N=10 bands are used: 412, 443, 488, 531, 555, 667, 678, 748, 869 and 1240 nm.

The 10-based logarithm of the chlorophyll concentration will be noted logC. The scheme is the following:

- Consider the following cost function
  f: (log$C_i, b_{bNC,i}) \rightarrow \epsilon_i$:
  1. For the current values of $logC_i$ and $b_{bNC,i}$, and for each wavelength λ among the N selected bands, calculate the water reflectance spectrum $\rho^+_{w\text{mod}}([chl]_i, b_{bNC,i}, \lambda)$ from the model described in section 4.2
  2. Calculate the values of c_0, c_1 and c_2 obtained by the polynomial fit for all bands $\lambda_1..\lambda_N$:

$$T_0(\lambda)c_0 + c_1\lambda^{-1} + c_2\lambda^{-4} \approx \rho'(\lambda) - t(\lambda)\rho^+_{wmod}([chl]_i, b_{bNC,i}, \lambda)$$

In matrix notation:

$$\begin{pmatrix}\rho'(\lambda_1)\\ \vdots \\ \rho'(\lambda_n)\end{pmatrix} - \begin{pmatrix}t(\lambda_1)\rho^+_w(\lambda_1)\\ \vdots \\ t(\lambda_n)\rho^+_w(\lambda_n)\end{pmatrix} = \underbrace{\begin{pmatrix}T_0(\lambda_1) & \lambda_1^{-1} & \lambda_1^{-4}\\ \vdots & \vdots & \vdots \\ T_0(\lambda_n) & \lambda_n^{-1} & \lambda_n^{-4}\end{pmatrix}}_{\Lambda}\begin{pmatrix}c_0\\ c_1\\ c_2\end{pmatrix}$$

Using the "pseudo-inverse" of matrix Λ, the coefficients c_i are given by:

$$\begin{pmatrix}c_0\\ c_1\\ c_2\end{pmatrix} = (\Lambda'\Lambda)^{-1}\Lambda'\begin{pmatrix}\rho'(\lambda_1) - t(\lambda_1)\rho^+_w(\lambda_1)\\ \vdots \\ \rho'(\lambda_n) - t(\lambda_n)\rho^+_w(\lambda_n)\end{pmatrix}$$

where Λ' is the transpose of matrix Λ.

Practically, the matrix $(\Lambda'\Lambda)^{-1}\Lambda'$ is calculated once for each pixel, because Λ varies with $T_0(\lambda_i)$ (which varies with the air mass) and with λ_i. (which also varies from detector to detector for MERIS; for MODIS, λ_i is fixed). This matrix does not need to be re-calculated after each iteration, because only $\rho^+_w(\lambda_i)$ varies after each iteration. Thus, the calculation of the coefficients c_i reduces to a matrix product.

  3. Calculate the chi-square value of the previous fit:

$$\epsilon_i = \frac{1}{N}\sum_{j=1}^{N}\frac{\left\{\frac{1}{t(\lambda_j)}\left[\rho'(\lambda_j) - T_0(\lambda_j)c_0 - c_1\lambda_j^{-1} - c_2\lambda_j^{-4}\right] - \rho^+_{wmod}([chl]_i, b_{bNC,i}, \lambda_j)\right\}^2}{\max\left(\rho^+_{wmod}([chl]_i, b_{bNC,i}, \lambda_j), \rho_{min}\right)}$$

Where a threshold ρ_{min} = 0.005 is applied at the denominator.

This function f: $(logC_i, b_{bNC,i}) \rightarrow \epsilon_i$: represents the mean square error between the atmosphere and residual sun glint reflectances and its polynomial fit. The objective is then to minimize f with respect to the parameters $logC$ and b_{bNC}.

- The final values of logC and b_{bNC} are obtained by a n-dimensional iterative minimization technique of the cost function f, using a simplex method known as AMOEBA (Nelder & Mead, 1965). This technique consists in constructing successive polygons with n+1 vertices, called simplexes, by replacing at each iteration the vertex with the highest value, in order to converge toward a local minimum of the function f. In our case, n=2 and the simplexes are triangles. The first iteration simplex is defined by initial values $logC_0$ = 0 and $b_{bNC,0}$ = 0, and initial steps $\Delta logC_0$ = 0.05 and $\Delta b_{bNC,0} = 5 \times 10^{-4}$. The stopping criterion of this scheme is a threshold on the size of the simplex: this size is defined as the average distance between the center of the simplex and its vertices. The value of this threshold has been set to 0.005.

When the stopping criterion is achieved, we obtain the final values of the parameters c_0, c_1 and c_2, chl and b_{bNC}. With the final values of the coefficients c_i, the spectrum of water reflectances $\rho_w^+(\lambda)$ is given by the following relationship:

$$\rho_w^+(\lambda) = \frac{\rho'(\lambda) - (T_0(\lambda)c_0 + c_1\lambda^{-1} + c_2\lambda^{-4})}{t(\lambda)}$$

These values represent the bidirectional reflectances, for the observation geometry $(\theta_s, \theta_v, \phi)$ considered at the time of the measurement; they will be normalized for bidirectional effects using f/Q table (Morel & Gentili, 1993), by assuming that the sun and sensor are positioned at nadir.

They are then normalized with respect to the sun at nadir and the sensor at nadir, using f/Q coefficients (Morel & Gentili, 1993):

$$\rho_{w,\text{norm}}^+(\lambda) = \frac{\frac{f}{Q}(\theta_s = 0, \theta_v = 0, \text{chl}, \lambda)}{\frac{f}{Q}(\theta_s, \theta_v, \phi, \text{chl}, \lambda)} \rho_w^+(\lambda)$$

Constraint on the backscattering coefficient

An analysis of the seasonal evolution of the mean water reflectances over the south pacific region has shown an anomalous evolution (Figure 5.a). The temporal evolution of the reflectance at 560 nm is expected to be flat, as is the case for MERIS and MODIS data processed by SeaDAS. The South Pacific Gyre corresponds to very clear (oligotrophic) waters, with extremely low chlorophyll concentrations. The same analysis

has been carried out for the north Atlantic region where a similar anomaly was not evidenced.

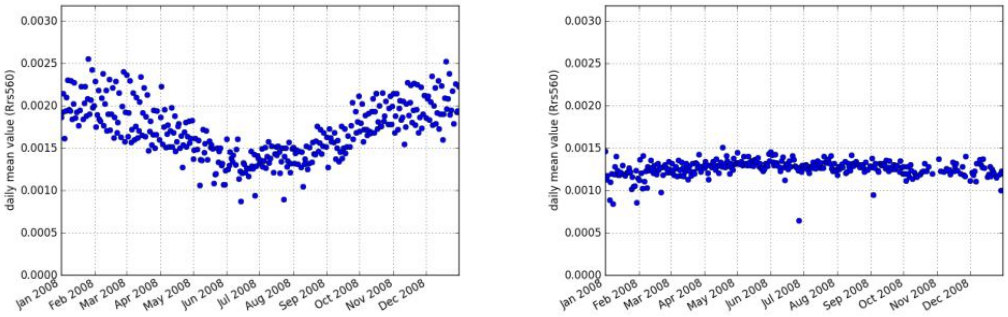

(a) (b)

Figure 5: Seasonal evolution of the mean reflectance at 560 nm over the South Pacific Gyre – without a constraint on the backscattering coefficient (a) and with a constraint (b)

The investigation of this problem has shown that there was in this case instability of the algorithm, probably due to an inaccuracy of the water model for clear waters. This instability manifests itself by anomalously high values of the retrieved backscattering coefficient b_{bNC}. To overcome this problem, a constraint on the backscattering coefficient is introduced: the backscattering coefficient is constrained to be close to zero, but only for very clear waters; this constraint is relaxed progressively with increasing chlorophyll concentrations. This is done by adding a supplementary term to the cost function ϵ_i defined previously. For a given chlorophyll concentration, the constraint is defined by a "width" defined as follows:

$$\sigma(\text{chl}) = \frac{\sigma_1^2}{\sigma_2} \exp\left(\ln\left(\frac{\sigma_1}{\sigma_2}\right) \log(\text{chl})\right)$$

Where log represents the logarithm to base 10 and ln the natural logarithm. This function increases exponentially with respect to log (chl), taking the values σ_1 = 0.0001 at chl = 0.01, and σ_2 = 0.005 at chl = 0.1. This function takes very large values at higher chlorophyll concentrations, so that almost no constraint will be applied in this chlorophyll concentration range.

Finally, the term $\epsilon_{\text{constraint}}$ added to ϵ_i depends on b_{bNC} and chl, and takes the form of a Gaussian the direction of b_{bNC}:

$$\epsilon_{\text{constraint}}\,(b_{bNC},\text{chl}) = A * (1 - \exp\,(-\frac{b_{bNC}^2}{2 \cdot \sigma(\text{chl})^2}))$$

where A = 0.001, $\sigma_1 = 1 \cdot 10^{-4}$, $\sigma_2 = 5 \cdot 10^{-4}$, and σ(chl) is defined previously.

4.4 Workflow

The workflow for the spectral matching process is presented on Figure 6:

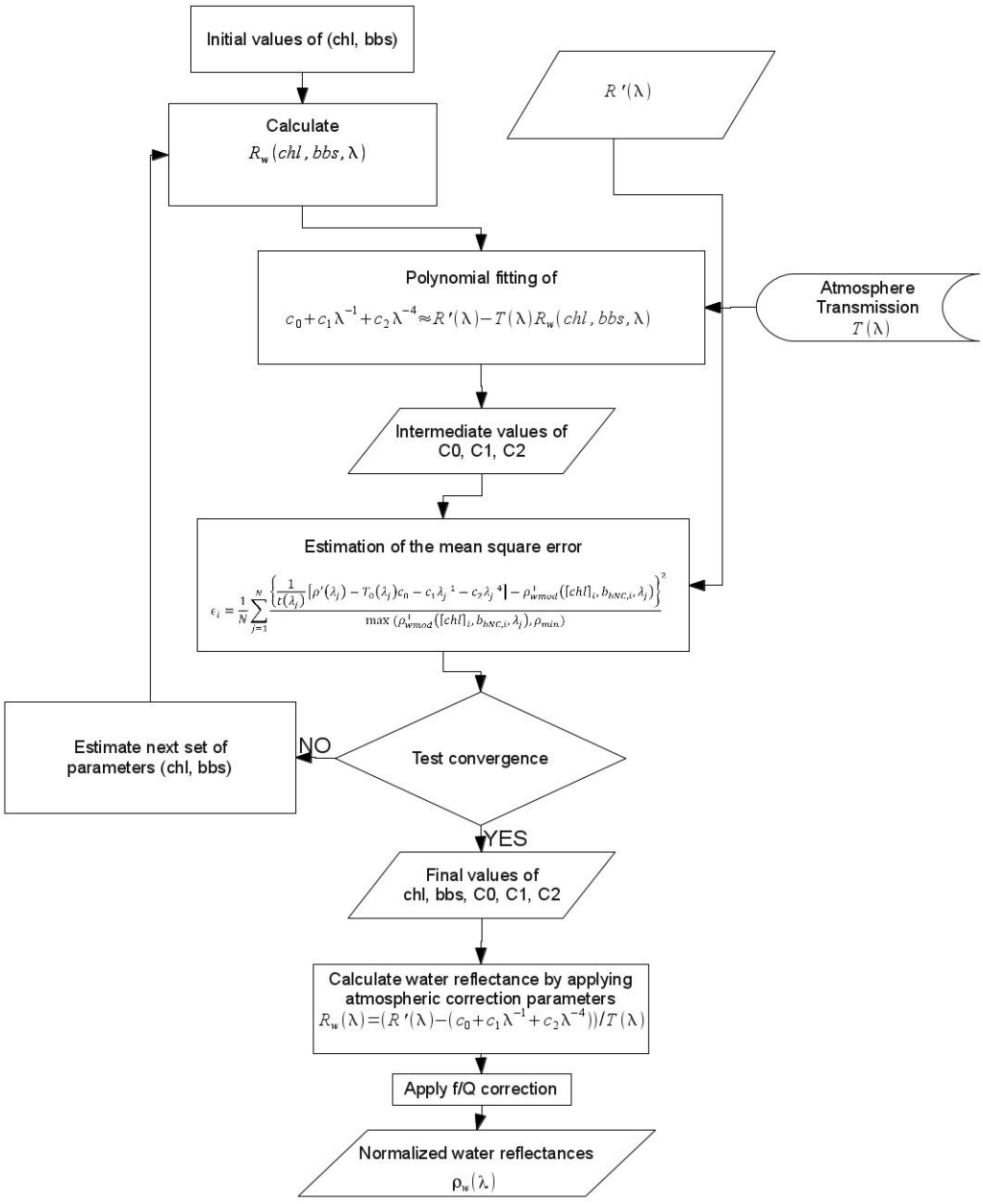

Figure 6: Workflow for the spectral matching process

5. SENSITIVITY STUDY

To estimate the theoretical accuracy and the characteristics of this algorithm, we have applied it to a synthetic dataset. This dataset has been generated by the SOS radiative transfer code, with ocean reflectances obtained by the model previously described. Only case 1 waters have been simulated (b_{bNC} = 0), and the chlorophyll concentrations range is 0.03 to 10 mg/m3 (12 values equally spaced in logarithmic scale). For each chlorophyll concentration, a combination of various atmospheric conditions has been simulated:

- Various observation geometries, including various sun glint conditions: 9 values of equally spaced relative azimuth angle ranging from 0 to 180°, two sun zenith angles (17.6° and 36.2°), and two view zenith angles (6.5° and 25.0°)
- Various aerosol optical thicknesses at 865 nm: 0., 0.01, 0.02, 0.05, 0.1, 0.2 and 0.4
- 12 aerosol models by Shettle and Fenn (Shettle & Fenn, 1979): M98, M95, M90, M80, C90, C80, C70, T99, T98, T90, T80, T70

The wind speed is set to 5 m/s, which determines the sun glint intensity from the Cox and Munk model.

For these conditions, three cases are considered: (1) a "mixed" case: ρ_{gli} < 10%, (2) a "no aerosol" case: τ_{aer} = 0, no limit on ρ_{gli} and (3) a "no glint" case: ρ_{gli} < 1%.

Then, noise has been optionally added to the synthetic values of TOA reflectances, with signal to noise ratios (SNR) typical of future Sentinel-3 instrument. The SNR values are wavelength dependent and also depend on the TOA radiances: the order of magnitude of SNR is about 700 in blue bands to about 400 in the NIR.

The resulting sets of TOA reflectances have been processed with POLYMER, and the simulated values are compared to the retrieved values. In a few particular conditions, the algorithm is unstable: this condition is the lowest chlorophyll concentration (0.03 mg/m3) and moderate to high glint condition (125 items out of 31248 in the "mixed" case). The algorithm then retrieves high chlorophyll concentration and negative values of b_{bNC}, which is not physically; these cases are flagged out. However, such instabilities have not been observed in realistic images, and these cases are removed from the comparison.

In this processing, the wind speed used for the initial molecular and sun glint correction is 7 m/s: this value is purposely set to be different from the value of 5 m/s used in the simulation, because the wind speed should not be considered to be known exactly. We have verified that if we use a wind speed of 5 m/s for this initial correction, and in absence of aerosol and additional noise, the simulation conditions are retrieved very well.

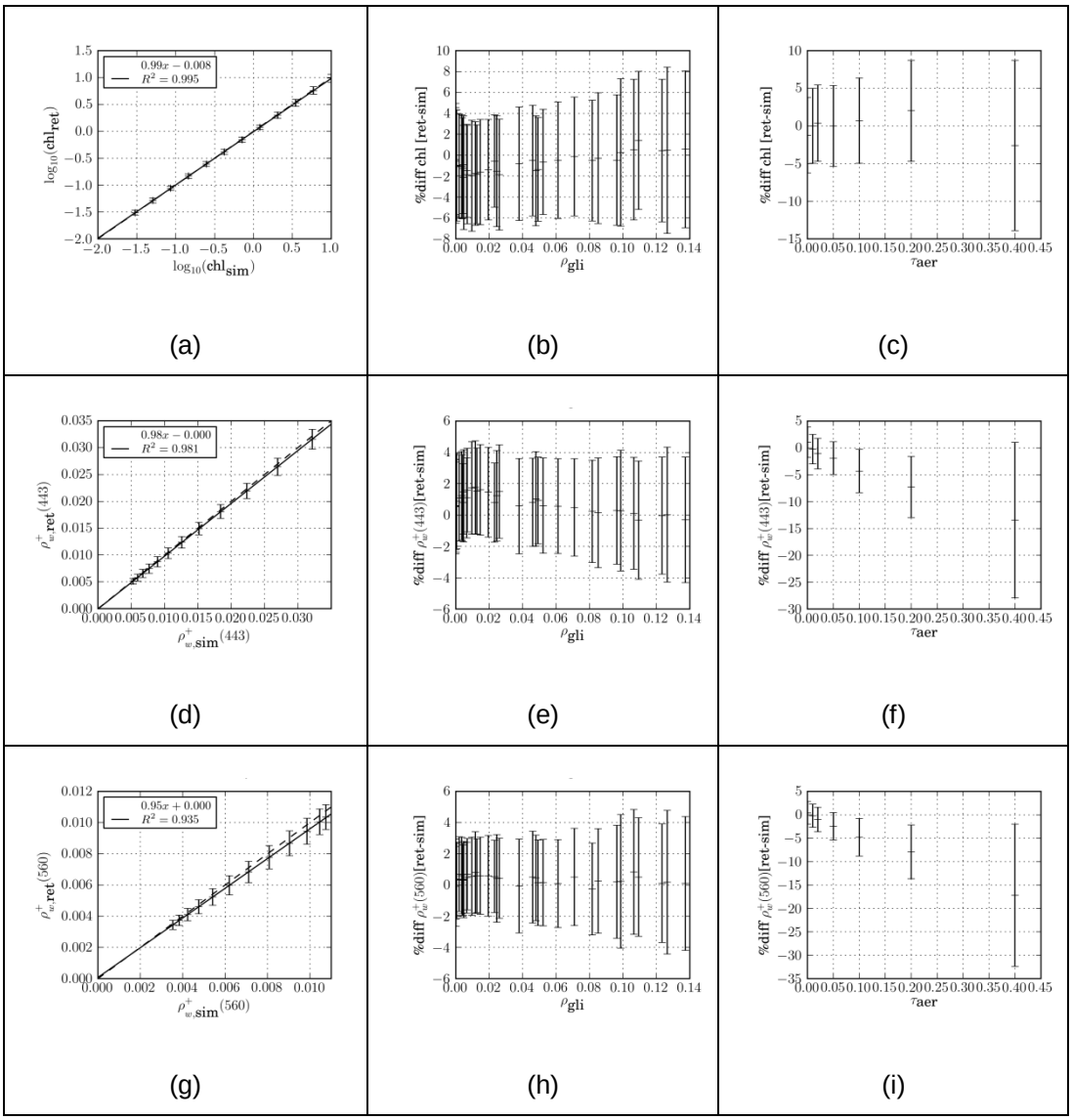

Figure 7: Plots for the comparison between the simulated parameters (synthetic dataset, indicated by subscript "sim"), and the parameters retrieved by POLYMER (indicated by subscript "ret"). In these figures, noise has been added to TOA reflectances according to typical Sentinel-3 SNR. Each row corresponds to the following parameters: chlorophyll concentration, water reflectance at 443 nm and 560 nm. The first column (Figs. (a), (d) and (g)) shows the regression between the synthetic and retrieved parameters, for the "mixed" case. The second column (Figs. (b), (e) and (h)) show the relative percent difference, between the retrieved and synthetic values ($\frac{\text{ret}-\text{sim}}{\text{sim}}$), as a function of the sun glint reflectance; emphasis is

put on the sun glint correction by using the case "no aerosol". The difference between $log_{10}(chl_{ret})$ and $log_{10}(chl_{sim})$ is multiplied by $ln(10)$ to convert to relative percent difference of the chlorophyll concentration ($\frac{\Delta chl}{chl} \approx ln(10)\Delta log_{10}(chl)$). The third column (Figs. (c), (f) and (i)) shows the relative percent difference, between the retrieved and synthetic values, as a function of the aerosol optical thickness at 865 nm; emphasis is put on the aerosol correction by using the case "no glint".

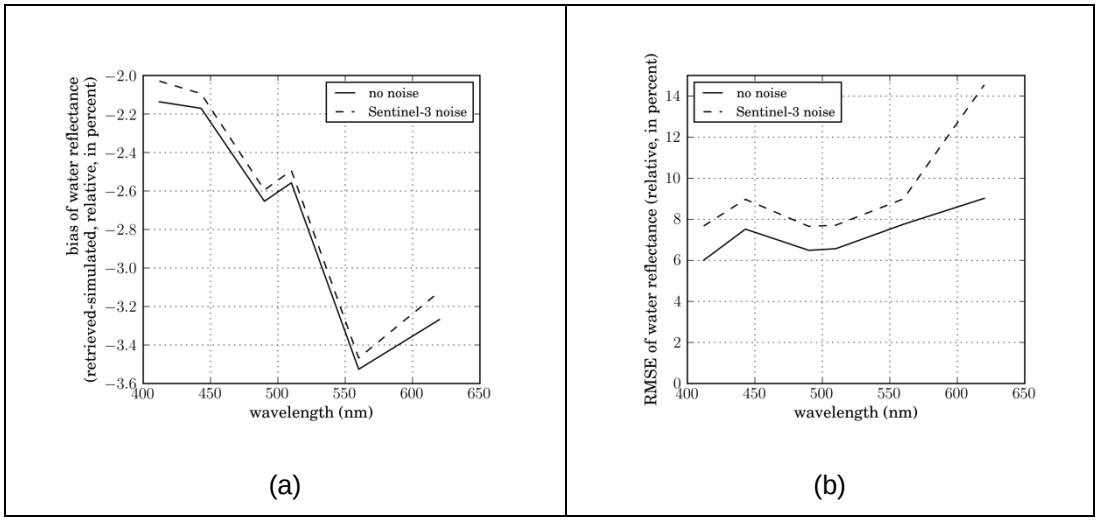

Figure 8: Summary of the relative precision (a) and accuracy (b) of the comparison between synthetic and retrieved water reflectances at each wavelength, for the "mixed" case, with and without noise added to TOA reflectances. GCOS recommends an accuracy of 5% on water reflectance in the blue and green bands.

The comparison between synthetic and retrieved data is presented on Figure 7. These figures include noise addition. For the "mixed" case (first column), we can see that the chlorophyll concentration is very well retrieved (R^2 = 0.995). The water reflectances at 443 and 560 nm are slightly biased low, but are still very well correlated with the simulations. The figures in the second column show the dependency between the error on each parameter and the sun glint intensity ("no aerosol" dataset). We can see that the retrieval of all parameters is almost independent of the sun glint intensity; the scatter increases only slightly with ρ_{gli} and no significant bias is observed. In particular, the water reflectances are retrieved with a bias lower than 1% and a RMSE lower than 5%, even in presence of a sun glint reflectance as high as 14%. The figures on the third column show the dependency between the error on each parameter and the aerosol optical thickness ("no glint" dataset). In this case, we can see larger errors and a negative bias on the water reflectances, which increase with the aerosol load: large aerosol plumes with optical thicknesses at 865 nm in the order or greater than 0.4 may be degraded.

However, the error on the chlorophyll concentration is lower than the error on the reflectances. More generally, the retrieval of chlorophyll concentration is more robust than the retrieval of water reflectances, which is also the case for traditional atmospheric correction methods.

Figure 8 (a) and (b) summarize the relative bias and RMSE of the comparisons between synthetic and retrieved reflectances at each wavelength. We can see that the retrieved values are slightly low biased (between 2 and 4\% bias on the water reflectances). The effect of the noise on the bias is negligible. We also notice that the RMSE increase with the added noise is very moderate: the RMSE increases by less than 2% at all bands except 670 nm (where the reflectances are very small), which is in complete agreement with typical requirements on ocean color products. The RMSE of the water reflectances due to the method is in the order of 6-8% for the "mixed" case. It is noteworthy that the selected dataset ("mixed" case) is not intended to be representative of real data, and does certainly exaggerate the frequency of "difficult cases" (especially, the presence of aerosols).

This application to synthetic data has permitted to quantify the residue of atmospheric correction, by focusing on the major unknown signals: the sun glint and the aerosol scattering. It has shown that the instrumental noise propagates very moderately from TOA to oceanic reflectances through the atmospheric correction process. Moreover, residual errors are observed even in absence of additional noise, which suggests some residual differences between the polynomial atmospheric model and the actual spectral signal. These residual errors appear to be more correlated with the presence of aerosols than with the sun glint contamination - the errors on the water reflectances are indeed very weakly correlated with intensity of the sun glint in absence of aerosols.

6. IMPLEMENTATION CONSIDERATIONS

6.1 Language, system and libraries

The Polymer algorithm is implemented in C++ under linux. 32 bits and 64 bits architectures are supported. It uses the following libraries:

Table 4: libraries used by Polymer

Library	Description	Usage
epr_api	Envisat Product Reader API Developped by Brockmann Consult, available at https://github.com/bcdev/epr-api	Read Envisat Products
gsl	GNU Scientific Library	AMOEBA Simplex minimization method Matrix product and inversion
hdf4	Hierarchical data format, version 4	Write HDF4 level2 (optional) Read MODIS level 1 Read NO2 climatology files
netCDF	Network Common Data Form	Write NetCDF level 2 (optional)

6.2 Computation time

The typical level 1 to level 2 processing time is about 25 min for a full MERIS orbit (15000x1121 pixels) on a single CPU (AMD Phenom II X4 940).

6.3 Input data

Polymer supports multiple sensors and input formats. The following input files are currently supported:

Table 5: List of Polymer input formats

Input file	Format	Ancillary data

MERIS level 1	ENVISAT format	Meteo and ozone data provided in level 1 files (ECMWF). No other ancillary data needed.
MODIS level 1b	HDF	NCEP meteorological ancillary data; EPTOMS ozone data (following SeaDAS: http://seadas.gsfc.nasa.gov/doc/toplevel/anc_info.html)
Text files	ASCII	Meteo and ozone data provided in the text files

Remark: Polymer supports input data provided in text files. This is useful for validation: level 1 data is extracted to ascii data for level 1 pixels co-located with validation data, which makes it possible to re-process a validation dataset very fast.

6.4 Output data

The level 2 products are written in a single hdf4 or netcdf4 file. It contains the following datasets:

Table 6: List of Polymer output datasets

	Dataset	Data type	Remarks
main parameters	latitude	float32	
	longitude	float32	
	logChl	float32	Chlorophyll concentration (mg/m3, in 10-based logarithm)
	bbNC	float32	backscattering coefficient of non-covarying particles
	Rw412	float32	Water reflectance above the surface, at 412 nm, normalized for θ_v = 0 and θ_s = 0
	⋮	⋮	⋮
	Rw865	float32	Water reflectance above the surface, at 865 nm, normalized for θ_v = 0 and θ_s = 0
	bitmask	uint16	quality flags

supplementary parameters	C0	float32	
	C1	float32	
	C2	float32	
	Rgli	uint16	Reflectance of the sun glint predicted from ECMWF wind speed
	R'865	uint16	TOA reflectance at 865 nm corrected for Rayleigh scattering

The parameters which have been used during the processing are stored in the level2 attributes. This includes, for example, the processor version, date of processing and processing parameters such as the spectral bands used.

7. REFERENCES

Ahmad, Z., McClain, C. R., Herman, J. R., Franz, B. A., Kwiatkowska, E. J., Robinson, W. D., et al. (2007). Atmospheric correction for NO2 absorption in retrieving water-leaving reflectances from the SeaWiFS and MODIS measurements. *Appl. Opt.*

Bricaud A., H. C. (1998). *Variations of light absorption by suspended particles with chlorophyll a concentration in oceanic (case 1) waters: Analysis and implications for bio-optical models.* Journal of Geophysical Research, v. 103, 31033-31044.

Buiteveld, H., Hakvoort, J., & Donze, M. (1994). Optical properties of pure water., *2258*, pp. 174-183.

Cox, C., & Munk, W. (1954). Measurement of the roughness of the sea surface from photographs of the sun's glitter. *J. Opt. Soc. Am., 44, 11, 838-850* .

D'Alba, L., & Colagrande, P. (2005). *MERIS smile effect characterization and correction.* techreport.

Fisher, J., & Grassl, H. (1991). Detection of cloud-top height from backscattered radiances within the oxygen A band. I, Theoretical study. *Journal of Applied Meteorology* .

Lenoble, J., Herman, M., Deuze, J., Lafrance, B., Santer, R., & Tanre, D. (2007). A successive order of scattering code for solving the vector equation of transfer in the earth's atmosphere with aerosols. *Journal of Quantitative Spectroscopy and Radiative Transfer 107, 479-507* .

Loisel, H., & Morel, A. (1998). Light scattering and chlorophyll concentration in case 1 waters: a re-examination. *Limnology and Oceanography. 43: 847-857.*

Morel, A. (1988). Optical modeling of the upper ocean in relation to its biogenous matter content (case I waters). *J. Geophys. Res., 93, 10749-10768* .

Morel, A., & Gentili, B. (1993). Diffuse reflectance of oceanic waters. II Bidirectional aspects. *Appl. Opt. , 32*, 6864--6879.

Morel, A., & Maritorena, S. (2001). Bio-optical properties of oceanic waters : a reappraisal. *J. Geophys. Res., 106(C4) : 7163-7180.*

Morel, A., Gentili, B., Claustre, H., Babin, M., Bricaud, A., Ras, J., et al. (2007). Optical properties of the clearest natural waters. *Limnol. Oceanogr. 52, 217-229* .

Nelder, J., & Mead, R. (1965). A Simplex Method for Function Minimization. *Computer Journal, vol 7, pp 308-313* .

Ramon, D., Cazier, L., & Santer, R. (2003). *The surface pressure retrieval in the MERIS O2 absorption: validation and potential improvements.* IGARSS.

Ruddick, K. G., Cauver, V. D., & Park, Y. J. (2006). Seaborne measurements of near-infrared water leaving reflectance: the similarity spectrum for turbid waters. *Limnol. Oceanogr., 51(2), 1167-1179* .

Shettle, E. P., & Fenn, R. W. (1979). Models for the aerosols of the lower atmosphere and the effects of humidity variations on their optical properties. *AFGL-TR-79-0214, No 676* .

Steinmetz F., P.-Y. D. (2011). *Atmospheric correction in presence of sun glint: application to MERIS.* Optics Express, Vol. 19, Issue 10, pp. 9783-9800.

End of Document